International Journal of Mechanical and Production Engineering Research and Development (IJMPERD)
ISSN(P): 2249-6890; ISSN(E): 2249-8001
Vol. 7, Issue 2, Apr 2017, 93-120

COMPARATIVE SPECTRUM ANALYSIS FOR VIBRATION IN A ROTATING MACHINE WITH MULTIPLE VARYING CONDITIONSFOR UNBALANCE FAULT AND CHECK FOR FREQUENCY PEAK DOMINANCE

ARKA SEN[1], MANIK CHANDRA MAJUMDER[2],
SUMIT MUKHOPADHYAY[3] & ROBIN KUMAR BISWAS[4]

[1,2,3] *Mechanical Engineering Department, National Institute of Technology Durgapur, West Bengal, India*

[4]*Condition Monitoring and Structural Analysis Department, Central Mechanical Engineering Research Institute, Durgapur, India*

ABSTRACT

In the current research paper a comparative analysis has been done based on FFT and cross power spectrum analysis for effective diagnosis of vibration in a rotating shaft with different unbalance conditions. The shaft has been rotated at different speed with different unbalance masses to gather enough information regarding the vibration characteristics of the system. Amplitude spectrum showed noise interferences whereas the cross power spectrum was accurate in predicting the frequency peaks and its amplitude. Also frequency peak dominancy for unbalance fault was established for higher RPM irrespective of the presence of other types of faults.

KEYWORDS: Condition Monitoring, Rotating Equipment Vibration, Fast Fourier Transform & Cross Power Spectrum

Received: Jan 28, 2017; **Accepted**: Mar 07, 2017; **Published**: Mar 15, 2017; **Paper Id**.: IJMPERDAPR201710

Original Article

INTRODUCTION

Rotor unbalance is the most common reason in machine vibrations. Most of the rotating machinery problem can be solved by using the rotor balancing and misalignment. Mass unbalance in a rotating system often produces excessive synchronous forces that reduce the life span of various mechanical elements. A very small amount of unbalance may cause severe problem in high speed rotating machines. The vibration caused by unbalance may destroy critical parts of the machine, such as bearings, seals, gears and couplings. Rotor unbalance is a condition in which the centre of mass of a rotating assembly, typically the shaft and its fixed components like disks and blades etc. is not coincident with the centre of rotation. In practice, rotors can never be perfectly balanced because of manufacturing errors such as porosity in casting, non-uniform density of material, manufacturing tolerances and gain or loss of material during operation. As a result of mass unbalance, a centrifugal force is generated and must be reacted against by bearing and support structures.

Vibration is a form of movement; in consequence, the relations between acceleration, velocity and displacement are governed by simple kinematics; acceleration is the derivative of velocity, which in turn is the derivative of displacement:

$$v(t) = \frac{dx(t)}{dt} \qquad a(t) = \frac{dv(t)}{dt}$$ Eq (1)

Conversely, displacement is the integral of velocity, which in turn is the integral of acceleration:

$$v(t) = \int_{t_0}^{t} a(\tau)d\tau + v(t_0) \qquad x(t) = \int_{t_0}^{t} v(\tau)d\tau + x(t_0)$$

Eq (2)

For an arbitrary vibration signal, the only way to convert one of these measures into another would be to know the complete time waveform and differentiate or integrate it. Fortunately, the integral and derivative of a sinusoidal function are also sinusoidal functions, so for sinusoidal waveforms these relations simplify to (the intermediary math has been omitted):

- **From Displacement to Velocity and Acceleration**

$$x(t) = X\cos(2\pi ft - \phi_x)$$

Eq (3)

$$v(t) = (2\pi f)X\cos\left(2\pi ft - \left(\phi_x - \frac{\pi}{2}\right)\right)$$

Eq (4)

$$a(t) = (2\pi f)V\cos\left(2\pi ft - \left(\phi_v - \frac{\pi}{2}\right)\right) = (2\pi f)^2 X\cos(2\pi ft - (\phi_x - \pi))$$

Eq (5)

- **From Acceleration to Velocity and Displacement**

$$a(t) = A\cos(2\pi ft - \phi_a)$$

Eq (6)

$$v(t) = \frac{1}{(2\pi f)}A\cos\left(2\pi ft - \left(\phi_a + \frac{\pi}{2}\right)\right)$$

Eq (7)

$$x(t) = \frac{1}{(2\pi f)}V\cos\left(2\pi ft - \left(\phi_v + \frac{\pi}{2}\right)\right) = \frac{1}{(2\pi f)^2}A\cos(2\pi ft - (\phi_a + \pi))$$

Eq (8)

It is important to observe that if one of the three variables —acceleration, velocity or displacement— is sinusoidal, the other two are also sinusoidal at the same frequency; only amplitude and phase change.

Phase Relations

Phase relations are fairly intuitive and independent of amplitude and frequency. The phase difference between acceleration and displacement is always 180°, which means that when the object reaches its maximum displacement from the equilibrium position, the acceleration is maximum in the opposite direction (see points 1 and 2 in the Figure below). Velocity always lags acceleration by 90° and leads displacement by 90°: it is maximum when both acceleration and displacement are zero, that is, when passing trough the equilibrium position (points 3 and 4).

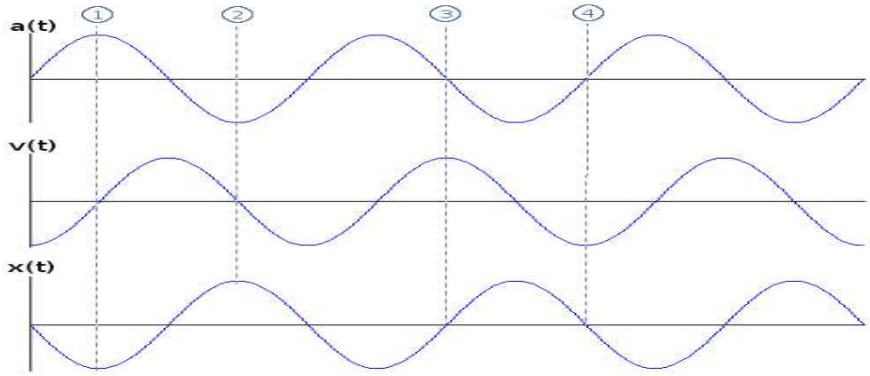

Figure 1: Phase Difference between Acceleration, Velocity and Displacement

Amplitude Relations

The amplitude of acceleration, velocity and displacement are related by factors that depend on vibration frequency. For a given velocity amplitude, for example, the corresponding displacement amplitude is higher at low frequencies by a factor proportional to 1/f and acceleration is higher at high frequencies, by a factor proportional to f. This relations explain why low frequency vibration is emphasized by displacement measures and high frequency vibration by acceleration, as illustrated in the following Figure 2: Sinusoidal acceleration and displacement amplitude as a function of frequency for a fixed velocity amplitude of 1 mm/s rms Units in this Figure were chosen because they are commonly used and to make the curves fit in the plot. If different units are used, the scale of the curves will vary but their general form remains the same.

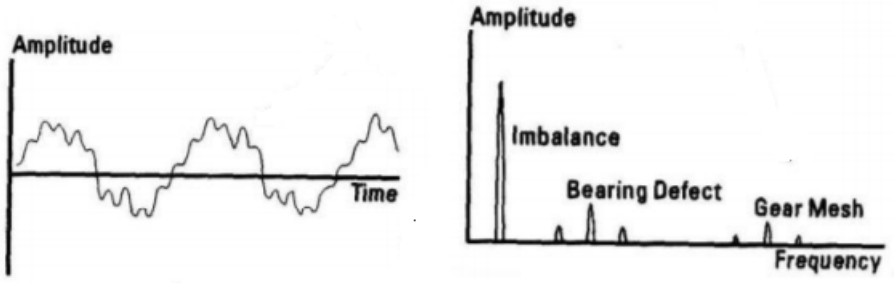

Figure 2: Time Domain and Frequency Domain

LITERATURE REVIEW

In the paper by **Jae Hong Suh (1)** used the vibration data from a gearbox as for the development of the Intelligent Diagnosis and Prognosis System by computing the wavelet coefficients using Morlet wavelet and Artificial Neural network as classification/decision making tool. **Peter W. Tse (2)** and **D.F Shia (3)** designed exact wavelet analysis to enhance the robustness of vibration-based machine fault diagnosis using Genetic Algorithm to reveal the time and frequency properties of the inspected signal. **B. Liu (4)** proposed a method to select the wavelet packet basis for fault diagnosis of rotating machinery by dividing the signal vector space into two subspaces and represented them in different ways containing the transient components excited possibly by localized defects and the other contains the remaining components. **H.X. Chen (5**) suggested adaptive wavelet transform (AWT) to model vibration signal using Morlet wavelet for diagnosis. The defect amplitudes and frequency component of the impulse vibration signal was extracted and displayed in the time–frequency plane. **Qiang Miao (6)** in his paper, have introduced Hidden Markov Model based two-stage

machine condition classification system based on wavelet modulus maxima. The modulus maxima distribution was used as the input sequence of the system. An adaptive algorithm was proposed and validated by three sets of real gearbox vibration data to classify two conditions: normal and failure. **Rui Zhou (7)** proposed redundant second generation wavelet packet transform for fault diagnosis of rotating equipment. Because the length of the coefficients at each level was equal to the length of raw signal after decomposition, the wavelet packet coefficients was able to retain more faulty information**. Cusido (8)** combined wavelet and power spectral density techniques to give the power detail density as a fault factor which combines the time-frequency analysis of wavelet decomposition allowing a further fault factor estimation. Based on the good shift-invariance and reduced aliasing properties of Dual Tree Complex Wavelet Transform **Yanxue Wang (9)**incorporated DTCWT with NeighCoeff shrinkage showed better performance than Discreet Wavelet Transform and Second Generation Wavelet Transform based methods for faulty detection and diagnosis of rotating machinery. **F. Al-Badour (10)** in his research work studied the application the Wavelet Packet Transform, to fault detection in rotating machinery**.** Failure of FFT techniques in detecting faults from non-stationary signals was mentioned in his study. **Lei Youa (11)** proposed a new type of fault diagnosis system of rotating machinery vibration signal, which can measure the vibration acceleration and velocity signals accurately, and analyse the vibration severity and frequency division amplitude spectrum of vibration signal. Based on wavelet and correlation filtering, **Shibin Wang (12)** proposed a technique incorporating transient modeling and parameter identification for rotating machine fault feature detection by which both parameters of a single transient and the period between transients was identified from the vibration signal, and localized faults was detected based on the parameters, especially the period. **Z.K Peng (13)** in his research developed the time–frequency data fusion (TFDF) technique by incorporating the idea of data fusion technique and by combining the results produced by two or more different TFA methods i.e. Short Time Fourier Transform and Continuous Wavelet Transform. The TFDF technique was more accurate time–frequency presentation for the target signal than that of any individual TFA method. **Md. Abdul Saleem (14)** found the 'Deflected Shape of Shaft' (DSS) of a rotating machine for detecting unbalance in its rotating components using Fast Fourier Transform (FFT) method. **B. Kiran Kumar (15)** in his paper measured the vibration velocities at five different speeds using FFT (Fast Fourier Transform) at initial condition. Based on vibration readings, spectrum analysis and phase analysis was carried out to determine the cause of high vibrations and later by observing the spectrum, unbalance was identified. **Bin Qiang Chen (16**) proposed a fast spatial–spectral ensemble kurtosis technique by incorporating discrete quasi-analytic wavelet tight frame (QAWTF) expansion methods were as the detection filters. **Jun Wang (17)** focussed on the improved time-scale representation by considering the non-linear property for effectively identifying rotating machine faults in the time-scale domain. He represented a new time-scale signature, called the Time Scale Manifold, by combining the Continuous Wavelet Transform and the non-linear manifold learning, for representing intrinsic machinery fault pattern, and explores the TSM ridge to identify the fault characteristic frequency. **Qingbo He (18)** combined the concepts of time–frequency manifold (TFM) and image template matching, and proposed a novel TFM correlation matching method to enhance identification of the periodic faults in a rotating machine. This method conducted the correlation matching of a vibration signal in the time–frequency domain by using the TFM with a short duration as a template. **Dongju Chen (19)** in his research work computed the frequency information for the spindle system, the V**Chen Bin Qiang (20)** proposed a pseudo wavelet system (PWS) based on the filter constructing strategies of wavelet tight frames to address the deficiencies of discreet wavelet transform which was implemented via a specially devised shift-invariant filter bank structure that generated non-dyadic wavelet sub bands as well as dyadic ones. **M. Lokesha (21)** presented automatic detection and diagnosis of gear condition monitoring technique using Laplace and Morlet wavelet based enveloped power spectrum. The time and frequency domain features extracted from Laplace wavelet based wavelet

transform are used as input to ANN for gear fault classification. Genetic algorithm was used to optimize the wavelet and ANN classification parameters. **Shibin Wang (22)** proposed a method based on transient modeling and parameter identification through Levenberg–Marquardt (LM) method for fault feature extraction of vibration signals. The double-side asymmetric model for the assigned problem was constructed based on parameterized Morlet wavelet, then the LM method was used to identify the parameters of the model. An iterative procedure was implemented to extract transients from the vibration signal, and eventually all extracted transients are represented in Time Frequency plane with satisfactory energy concentration, and there is no interference of cross- term among different transients. **Y. Yang (23)** proposed the procedure for procedure for the parameterized Time Frequency Analysis (TFA) to analyse the non-stationary vibration signal of varying-speed rotary machinery. The proposed method adopted the adaptive STFT to initialize the parameters estimation, and applied the spectrum concentration index to estimate the transform parameters. The estimated parameters are then used in component separation and parameterized TFA so the time–frequency features. **Adrian D. Nembhard (24)** discussed the transferability of the Individual Speed Individual Foundation (ISIF) and Multi Speed Individual Foundation (MSIF) techniques on a wider range of rotor related faults on different machines. A new Multi-Speed Multi-Foundation (MSMF) method which facilitates Fault Diagnosis by the direct comparison of vibration data from similarly con Figure machines with different dynamic characteristics operating at different steady-state speeds has also been proposed. **Wei Li (25**) in his paper used statistical feature extraction and evaluation method. The statistical features were sampled average of some conventional features, and these conventional features were obtained by analysing arbitrarily selected partitions of a given vibration signal with existing signal processing tools. According to the central limit theory, the obtained statistical feature vectors were close to normal distributions, and their means and variances could be estimated. The statistical features, the performance of ANN and SVM based fault classifiers was significantly improved. **Hocine Bendjama(26)** in his papers discussed fault diagnosis of rotating machinery using a combination between Wavelet Transform (WT) and Principal Component Analysis (PCA) methods. The WT was used to segregate the vibration signal of measurements data in different frequency bands. The obtained segregated levels were used as input parameters to the PCA method for fault detection and diagnosis**. Phadatare H. P (27)** in his paper describes how to calculate the nonlinear frequencies and resultant dynamic behaviour of high speed rotor bearing system with mass unbalance. Time history and FFT analysis were established for finding the fundamental frequencies for the rotating under variation of shaft diameter, effect of geometric nonlinearity and disk location while dynamic impact of mass unbalanced on the behaviour of rotor bearing system has been investigated using time history. Table 2 summarises the different Time Frequency methods used in condition monitoring.

GOVERNING EQUATIONS

A **fast Fourier transform** (**FFT**) is an algorithm that computes the discrete Fourier transform (DFT) of a sequence, or its inverse. Fourier **analysis** converts a signal from its original domain (often time or space) to a representation in the frequency domain and vice versa.

Fourier Transform (FT) is widely used in signal processing in terms of Fast Fourier Transform (FFT) as it is a powerful tool that allows one to analyse a particular signal in the frequency domain. The idea of fourier transform was first put forth by the French mathematician and physicist Jean Baptiste Joseph Fourier. If f(t) is a time domain

$$F(f) = \int_{-\infty}^{\infty} f(t) e^{-i2\pi ft} dt$$

Eq (9)

function(signal) then the frequency spectrum F(f) of this function using Fourier transform, assumed that it exists is given by,

In FFT or DFT, computations are based on the assumption that the data sampled over a time period are repeated before and after data measurement.

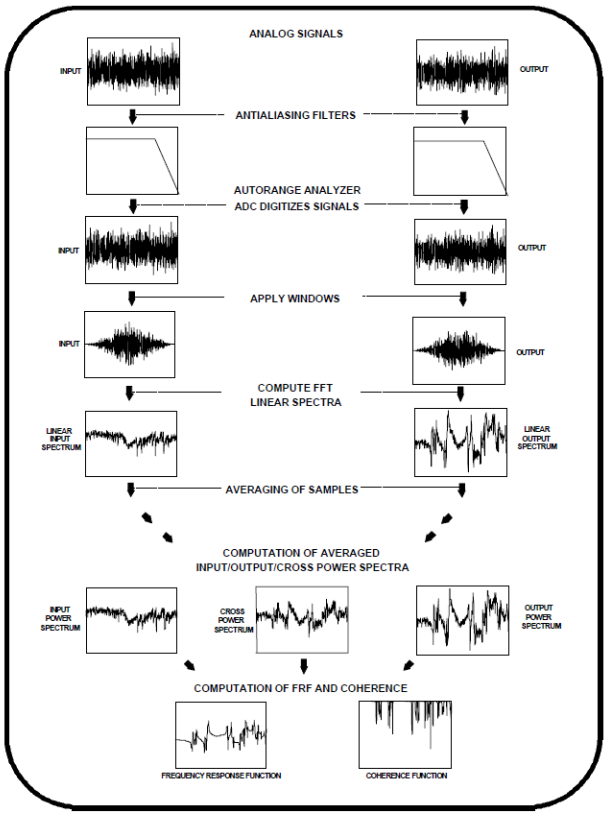

Figure 3: Anatomy of FFT Process

The FFT does not directly give you the spectrum of a signal. FFT can vary dramatically depending on the number of points (N) of the FFT, and the number of periods of the signal that are represented.. The FFT contains information between 0 and fs (sampling frequency), however, we know that the sampling frequency must be at least twice the highest frequency component. Therefore, the signal's spectrum should be entirely below fs, the Nyquist frequency. Recall also that a real signal should have a transform magnitude that is symmetrical for positive and negative frequencies. So instead of having a spectrum that goes from 0 to fs, it would be more appropriate to show the spectrum from − fs to fs. Cross spectral analysis allows one to determine the relationship between two time series as a function of frequency. Normally, one supposes that statistically significant peaks at the same frequency have been shown in two time series and that we wish to see if these periodicities are related with each other and, if so, what the phase relationship is between them. Suppose we have two time series x(t) and y(t) and we want to look for relationships between them in particular frequency bands. First consider harmonic analysis in terms of line spectra

$$x = \bar{x} + \sum_{k=1}^{n/2-1} \left(A_{xk} \cos\left(\frac{2\pi kt}{T}\right) + B_{xk} \sin\left(\frac{2\pi kt}{T}\right) \right) + A_{xN/2} \cos\left(\frac{\pi Nt}{T}\right)$$

Eq (10)

$$y = \bar{y} + \sum_{k=1}^{n/2-1}\left(A_{yk}\cos\left(\frac{2\pi kt}{T}\right) + B_{yk}\sin\left(\frac{2\pi kt}{T}\right)\right) + A_{yN/2}\cos\left(\frac{\pi Nt}{T}\right)$$

Eq (11)

Because of the orthogonality of the functions for evenly spaced data we can write the covariance between them as a sum of contributions from particular frequencies.

$$\overline{x'y'} = \frac{1}{2}\sum_{k=1}^{\frac{N}{2}-1}\left(A_{xk}A_{yk} + B_{xk}B_{yk}\right) + A_{x\,N/2}A_{y\,N/2}$$

Eq (12)

$$= \sum_{k=1}^{\frac{N}{2}} CO(k)$$

= Spectrum of x and y

EXPERIMENTAL SETUP AND PROCEDURE OF DATA COLLECTION

Considering the main cause of rotating machine vibration as unbalance, a test rig for experimental validation of the model based identification technique was built. Schematic representation of the experimental set has been shown in the Figure below.

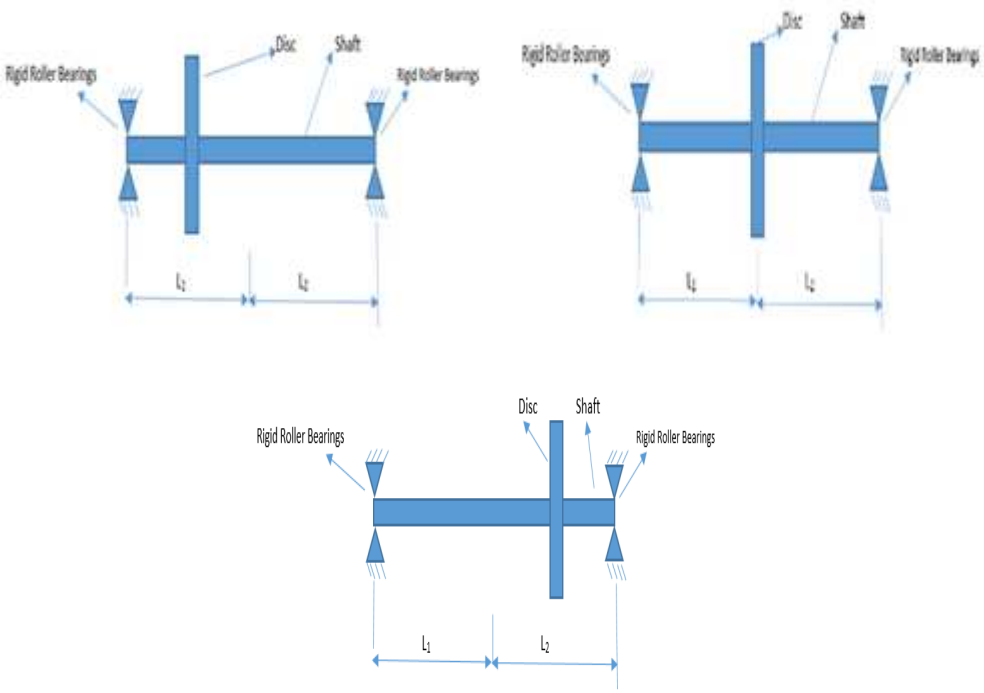

Figure 4: Schematic Representation of the Experimental Set up (No Fault Case)

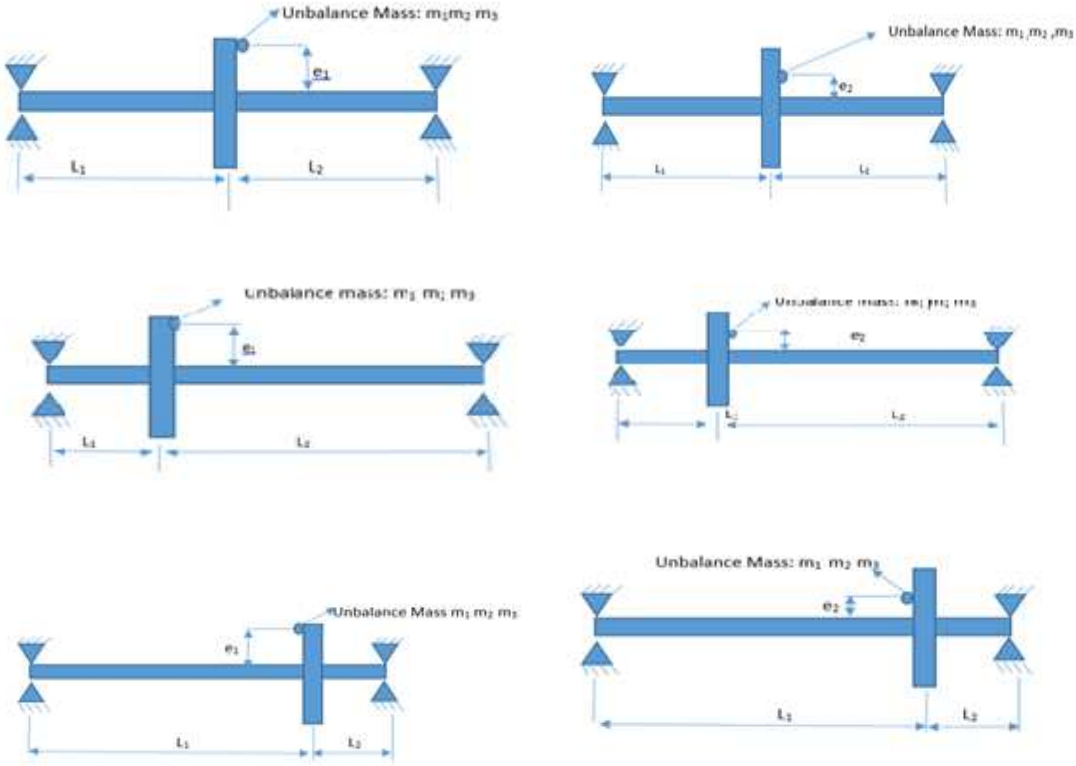

Figure 5: Schematic Representation of the Experimental Set up (With Unbalance Fault)

The experimental verification for the Unbalance Identification of mass on a shaft with single plane and two eccentricities has been performed on a Machine Fault Simulator provided at Central mechanical Engineering Research Institute (CSIR-CMERI) located at Durgapur.

A rigid shaft considered to be mass less is mounted between two roller bearings. The distance between the two bearings is L_1+L_2, which is 60cm. This shaft is connected to a Variable Frequency Drive (VFD) motor by a flexible coupling. To measure the vibration in X-Direction and Y-Direction at the two bearings, four accelerometers are connected; two in each bearing. The weight of the disc is 653 gram (M_1). The position of the disc is varied in three different locations: (i) 15 cm from left bearing (ii) 30cm from left bearing which is the mid position on the shaft (iii) 45 cm from left bearing. Initially no unbalance mass was attached in order to get the no fault readings. Three unbalance masses of 8 gram (m_1), 12 gram (m_2) and 16 gram (m_3) are attached subsequently to the disc at eccentricities 6.85cm (e_1) and 6.85cm (e_2) separately one by one. Then the shaft is rotated at rpm 300, 600, 900, 1200 and 1500; and simultaneously the vibration readings (RMS values) and their phase values in x and y-direction at the two bearings were noted down. Artificial Neural Networking Techniques with varying training algorithms have been used to determine the unbalance plane of vibration.

Figure 6: Unbalance Mass of 8gram Attached to the Rotating System

Figure 7: Unbalance Mass of 10gram Attached to the Rotating System

Figure 8: Unbalance Mass of 10gram Attached to the Rotating System

Eccentricity

All rotors have some eccentricity. Eccentricity is present when geometrical center of the rotor and the mass center do not coincide along their length. In the present case, the disc is considered absolutely balanced where the Geometrical Centre of the disc coincides with the Centre of the Gravity of the disc. In the current research work eccentricity is the distance between the Geometrical Centre (Centre of rotation) and the points where the unbalance mass is to be attached. There are two locations at a distance of 6.85cm from the centre of rotation (e_1) and at a distance of 4.85cm from the centre of rotation of the disc (e_2).

Figure 9: The Rotating Disc

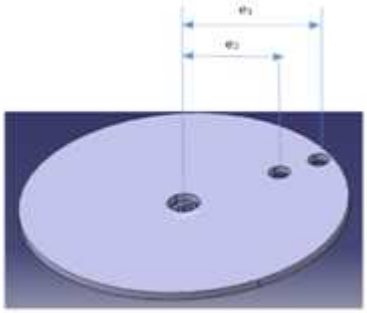

Figure 10: Schematic Representation of Rotating Disc

Plane of Unbalance

The Figure11, Figure12 and Figure 13 shows the different position of the rotating disc placed on the shaft.

Figure 11: Machine Fault Simulator with Rotating Disc Placed at Right Position

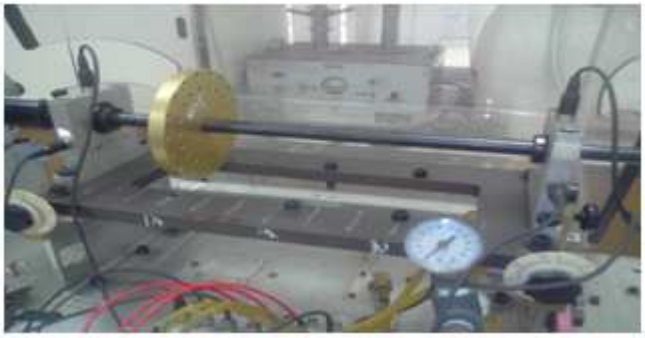

Figure 12: Machine Fault Simulator with Rotating Disc Placed at Left Position

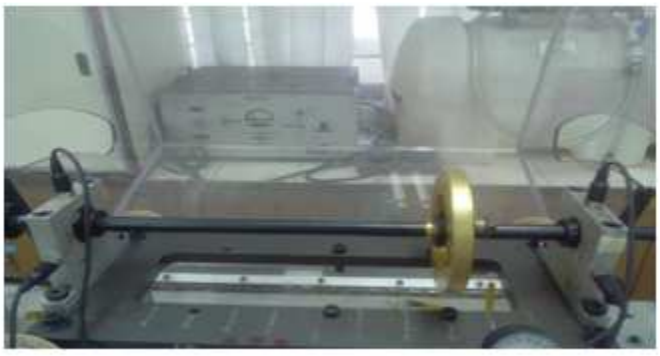

Figure 13: Machine Fault Simulator with Rotating Disc Placed at Right Position

The design of experiment (Table 2) is based on the maximum possible combination of Unbalance mass (m), Eccentricity (e), Plane of unbalance (p) and the RPM (r) values. The table (Table 1) below provides the maximum and minimum values the independent parameters/input to the system.

Table 1: Independent/Input Parameters and their Levels

SERIAL NO	INDEPENDENT /INPUT PARAMETERS	MINIMUM LEVEL	MAXIMUM LEVEL
1	Unbalance Mass (m)	8gram	16gram
2	Eccentricity (e)	4.85cm	6.85cm
3	Plane of unbalance (p)	15cm (measured from left bearing)	45cm (Measured from Left Bearing)
4	Revolutions per Minute (RPM) (r)	300	1500

Table 2: Design of Experiment

SET	EXPERIMENTAL CODES	UNBALANCE MASS (IN GRAM)	ECCENTRICITY (IN CM)	LOCATION OF UNBALANCE PLANE (IN CM) *(FROM LEFT BEARING)*
1	NFL	0	0	15
2	NFC	0	0	30
3	NFR	0	0	45
4	L8e2	8	4.85	15
5	C8e2	8	4.85	30
6	R8e2	8	4.85	45
7	L8e1	8	6.85	15
8	C8e1	8	6.85	30
9	R8e1	8	6.85	45
10	L12e2	12	4.85	15
11	C12e2	12	4.85	30
12	R12e2	12	4.85	45
13	L12e1	12	6.85	15
14	C12e1	12	6.85	30
15	R12e1	12	6.85	45
16	L16e2	16	4.85	15
17	C16e2	16	4.85	30
18	R16e2	16	4.85	45
19	L16e1	16	6.85	15
20	C16e1	16	6.85	30
21	R16e1	16	6.85	45

The design of experiment as mentioned in the table 2 has been performed for 300, 600, 900, 1200 and 1500 RPM`s. In total there are 105 set of experiments.

INDICATORS USED IN EXPERIMENT

NFC: No fault disc at Center, **NFL**: No fault disc at Left position, **NFR**: No fault disc at Right position

The number succeeding NFC, NFL, NFR represents the rpm at which the disc is rotating without any unbalance mass attached. With unbalance mass attached, the experimental code is written in the following format as mentioned below one after the other.

Position of Rotating Disc (p)⟶ Unbalance Mass (m)⟶ Eccentricity (e)⟶ Revolutions Per Minute (RPM) (r)

For Example: C16e11500 represents the rotating disc placed at centre of the shaft with mass unbalance of 16gram placed at an eccentricity e_1 rotated at 1500 RPM. It is similar for rest of the experimental cases.

RESULTS AND DISCUSSSIONS

In the present paper analysis has been done only with one disc at the center position of the shaft. Figure 14 to Figure 45 represents the cross power spectrum of vibration for all the different possible combination of unbalance mass, eccentricity, plane of unbalance and RPM.

CROSS POWER SPECTRUM ANALYSIS (AT RPM 300) LEFT BEARING X-DIERCTION (LX)

Figure 14: NFC300

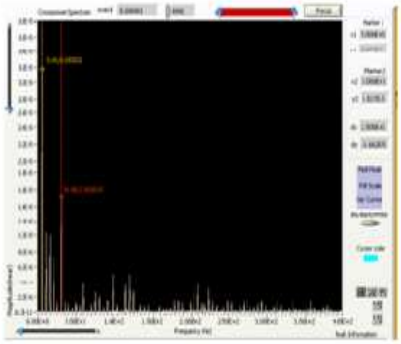

Figure 15: C8E1300

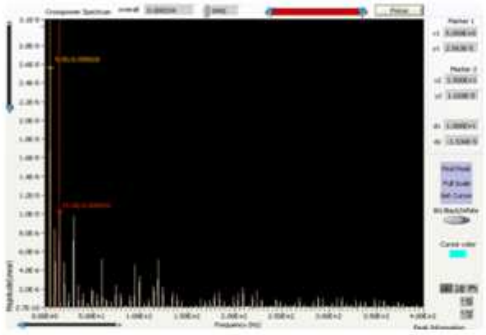

Figure 16:C12E1300

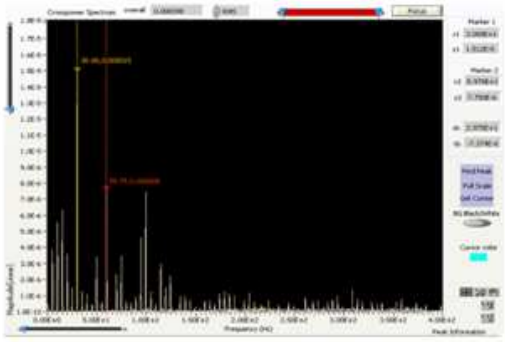

Figure 17:C16E1300

LEFT BEARING Y-DIERCTION (LY)

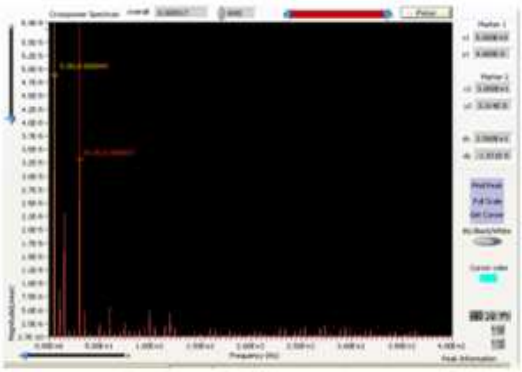

Figure 18: NFC300

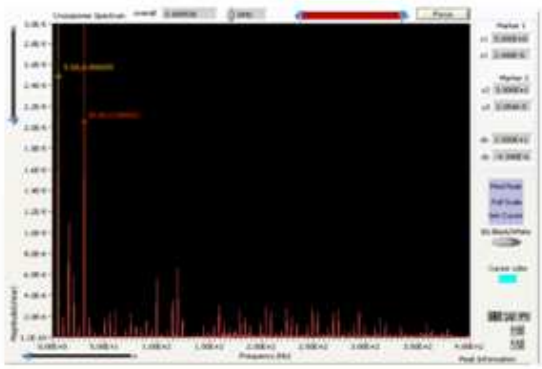

Figure 19:C8E1300

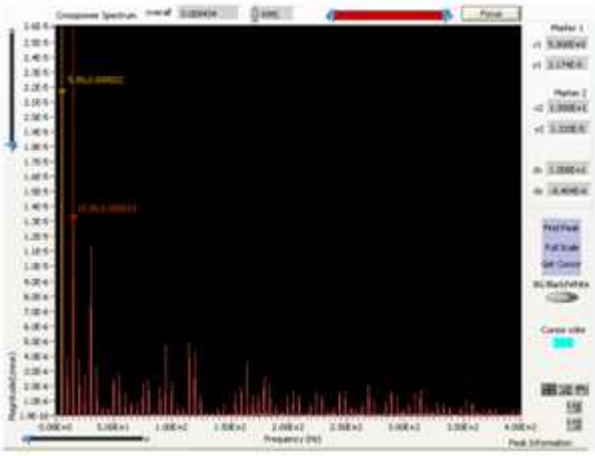

Figure 20: C12E1300

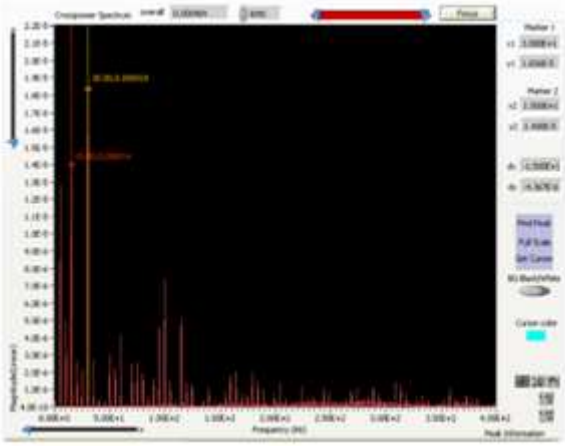

Figure 21: C16E1300

The analysis of the cross power spectrum for the rotation at 300 RPM reveals that for Left bearing X-direction frequency peaks for no fault case are shown at 5 HZ and 10 Hz (Figure 14). The peak at 5 Hz resembles residual unbalance whereas the peak at 10Hz indicates presence of misalignment (Figure 15). Frequency peaks were shown at 5Hz and 15Hz (Figure 16) indicating 1X and 3X rpm peaks for unbalance and misalignment respectively. In Figure 17 peaks were shown at 30Hz and 59.75 Hz which 6X and 12X RPM peaks which dominates the unbalance peaks due to higher impact of misalignment and bearing faults on the spectrum when the unbalance weight has been increased. Similarly for Left Bearing Y direction peaks at 1X RPM and 6X RPM were noticed for no fault case (Figure 18) and 8 gram unbalance mass attached (Figure: 19). 1X RPM and 3X RPM peak were noticed for 12 gram unbalance mass attached (Figure 20).3X RPM and 6X RPM peak were noticed for 16 gram unbalance mass attached(Figure 21).

RIGHT BEARING X-DIERCTION (RX)

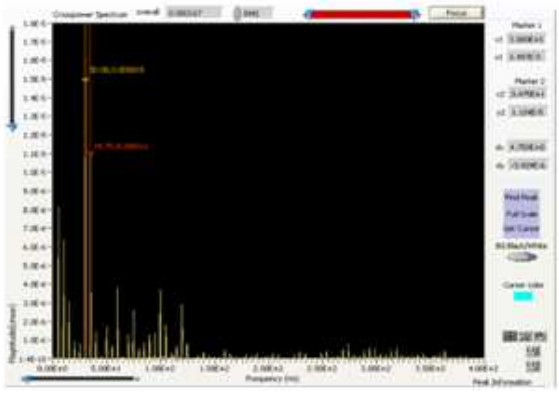

Figure 22: NFC300

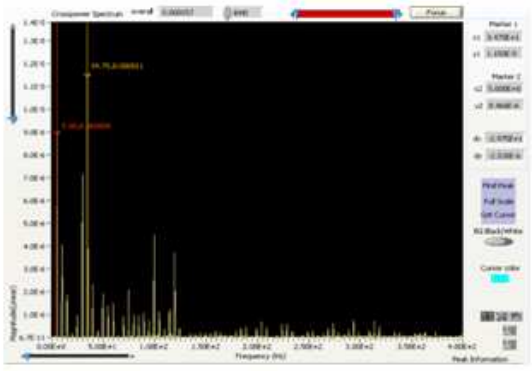

Figure 23: C8E1300

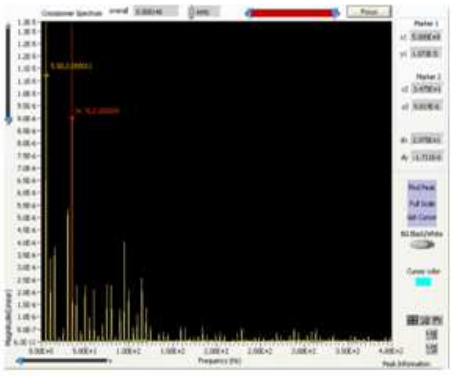

Figure 24: C12E1300

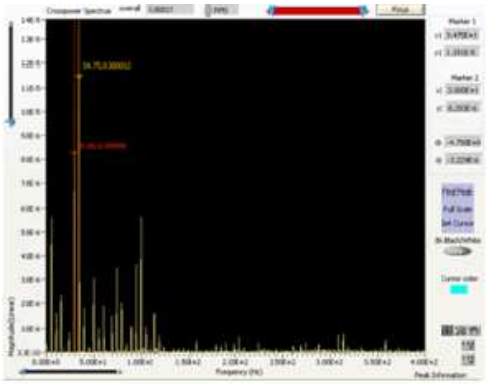

Figure 25: C16E1300

RIGHT BEARING Y-DIERCTION (RY)

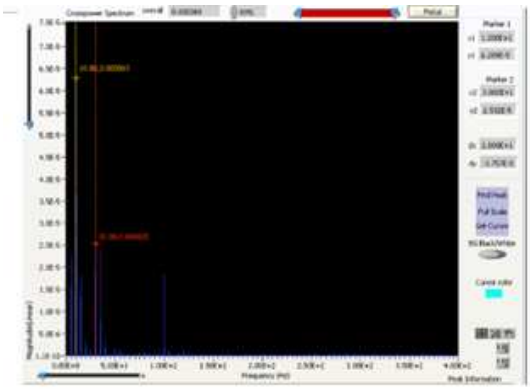

Figure 26: NFC300

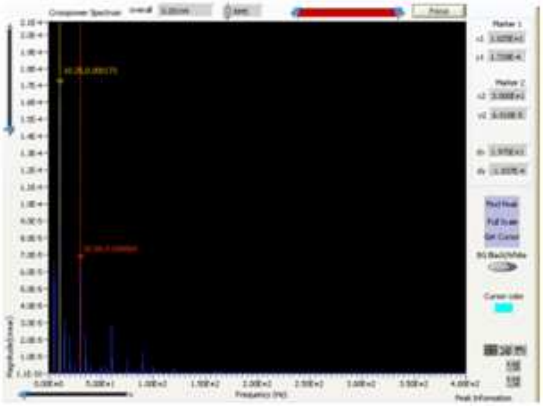

Figure 27: C8E1300

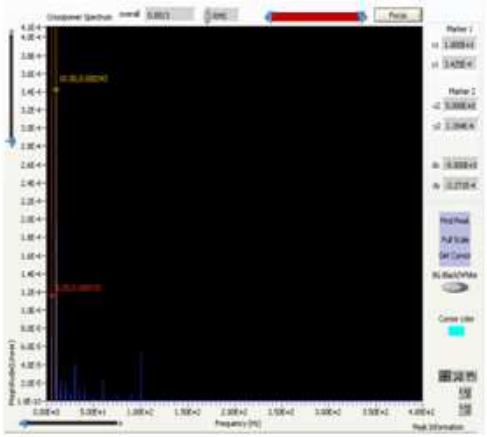

Figure 28: C12E1300

Figure 29: C16E1300

For Right Bearing X-direction peaks were observed at 6X and 7X RPM for no fault case (Figure 22). When unbalance masses of 8 gram and 12 gram was attached separately, peaks were observed at 1X and 7X RPM (Figure 23 and Figure 24) which indicates unbalance and bearings faults. The bearing faults dominates the unbalance fault in the case of 8 gram unbalance whereas in case of 12 gram unbalance the unbalance fault dominates the bearing faults. When 16 gram unbalance mass is attached, peaks were observed at 6X and 7X rpm indicating that the effect of bearing fault is much higher than the unbalance and the misalignment faults (Figure 25). For Right Bearing Y- direction in case of no fault and

when 8gram unbalance mass is attached, peaks were observed at 2X and 6X rpm indicating that the effect of misalignment and bearing fault is much higher than that of the unbalance fault (Figure 26 and Figure 27). For 12 gram and 16gram unbalance mass attached, the effect of misalignment is much more than that of the unbalance which is clearly shown by the peaks at 1X and 2X RPM (Figure 28 and Figure 29).

AT RPM 1500

LEFT BEARING X-DIERCTION (LX)

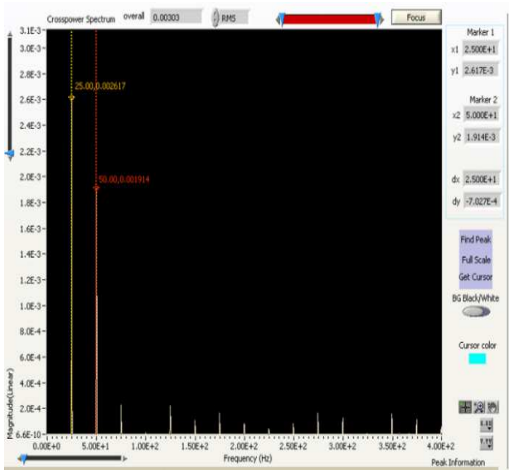

Figure 30: NFC1500

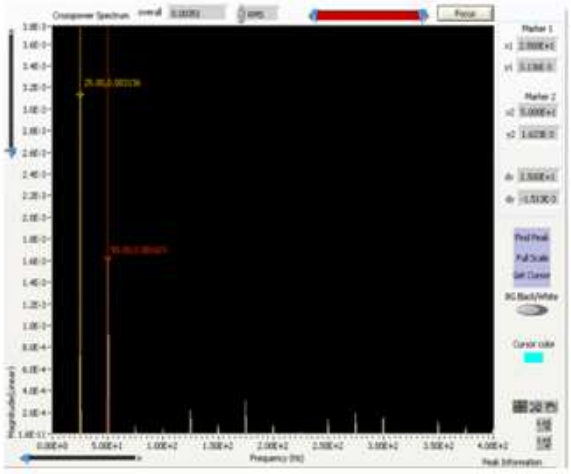

Figure 31: C8E11500

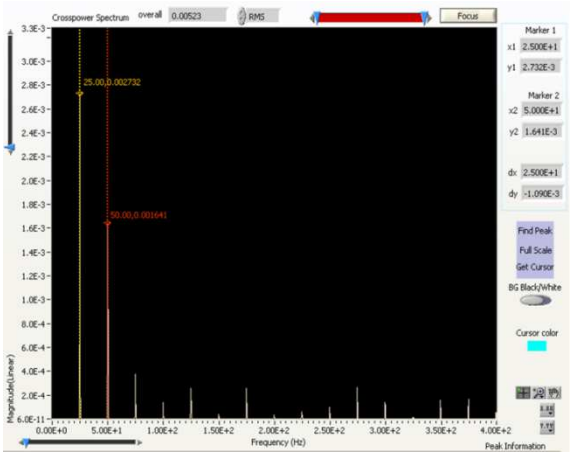

Figure 32: C12E11500

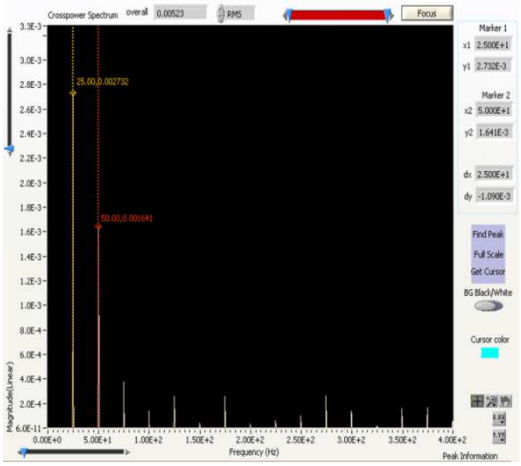

Figure 33: C16E11500

LEFT BEARING Y-DIERCTION (LY)

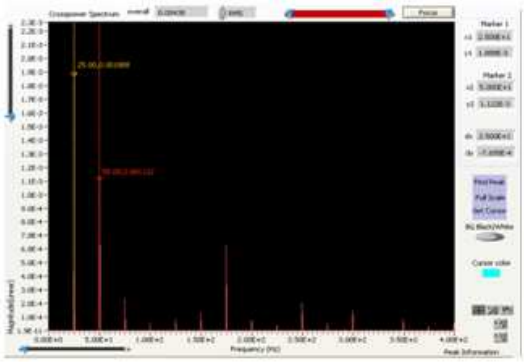

Figure 34: NFC1500

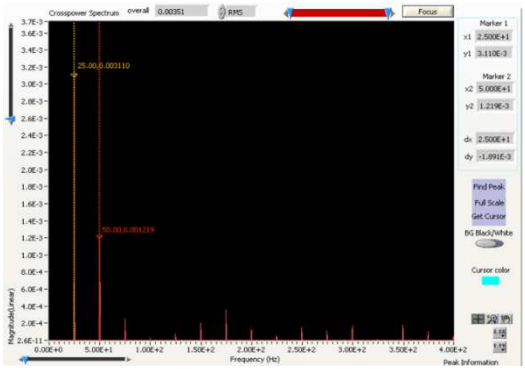

Figure 35: C8E11500

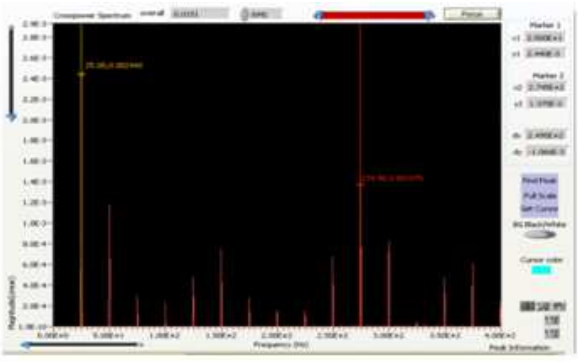

Figure 36: C12E11500

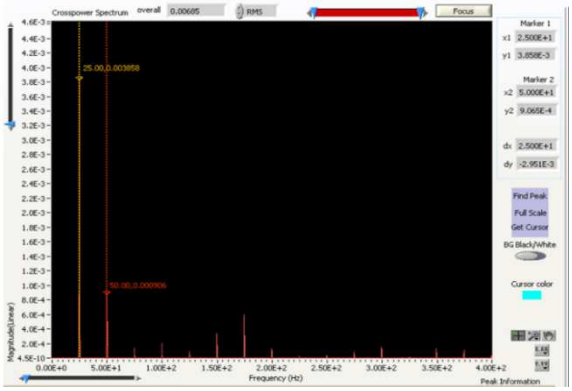

Figure 37: C16E11500

For 1500 RPM, the unbalance peaks and misalignment peaks were observed at 1X and 2X Rpm (25Hz and 50Hz) for no fault, 8gram, 12 gram and 16 gram unbalance for Left Bearing X-direction as shown in Figure 30, Figure 31, Figure 32 and Figure 32 respectively. For Left Bearing Y-direction the unbalance peaks were observed at 1X RPM for no fault, 8 gram, 12 gram and 16 gram unbalance as shown in Figure 30, Figure 31, Figure 32 and Figure 33. Peaks at 2X rpm were observed for misalignment in case of no fault case, 8 gram and 12 gram unbalance mass attached as can be seen in Figure 34, Figure 35, Figure 36. In Figure 37 the second dominant peak after the unbalance peak is at a very high frequency indicating some bearing fault.

RIGHT BEARING X-DIERCTION (RX)

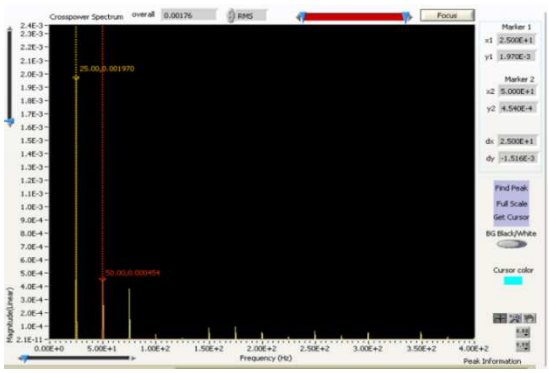

Figure 38: NFC1500

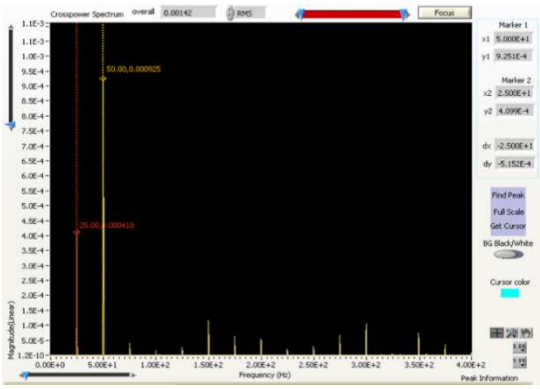

Figure 39: C8E11500

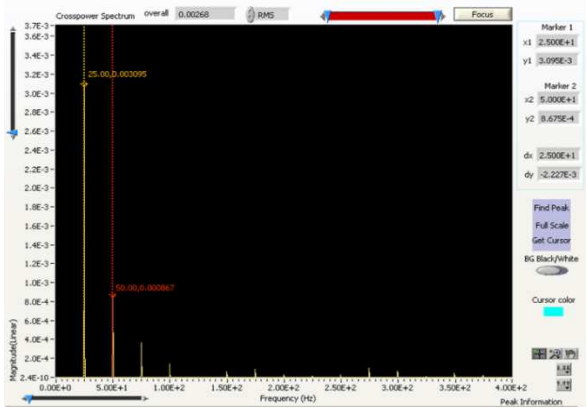

Figure 40: C12E11500

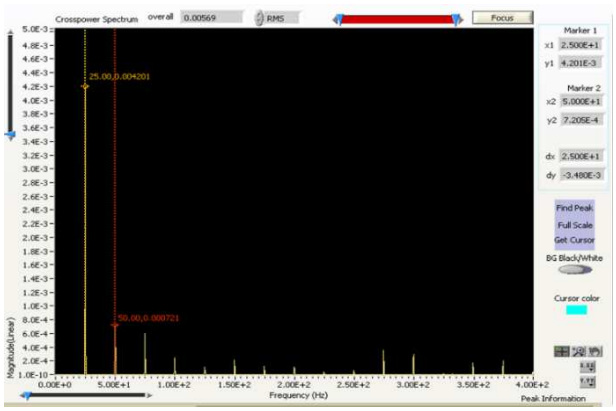

Figure 41: C16E11500

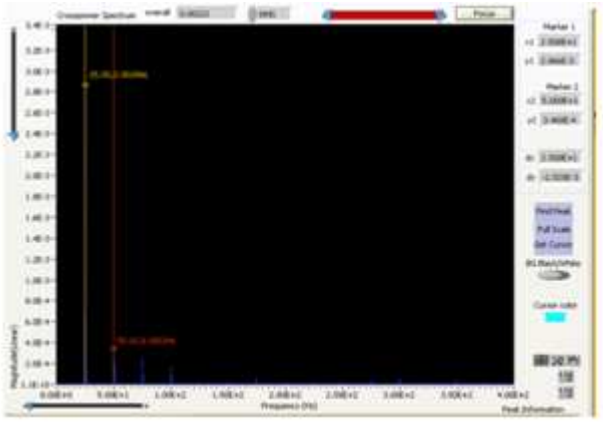

Figure 42: NFC1500

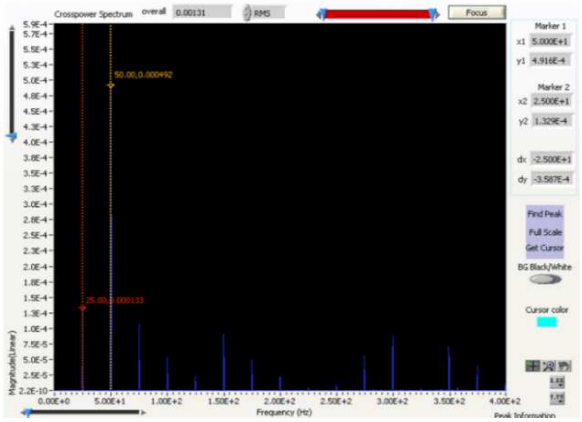

Figure43: C8E11500

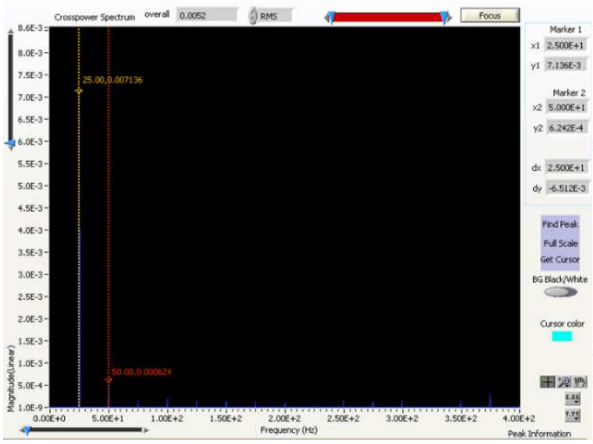

Figure 44: C12E11500

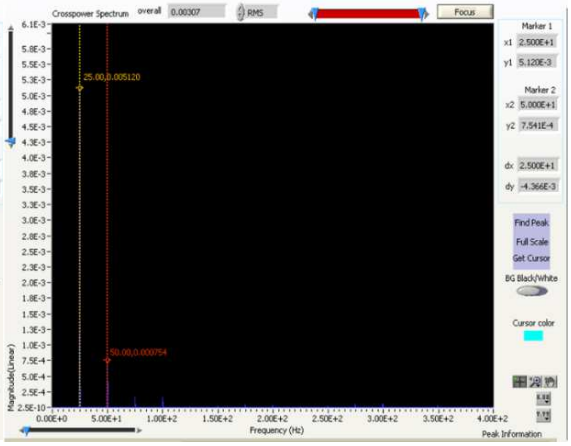

Figure 45: C16E11500

For Right Bearing X-direction unbalance peak at 1X RPM is shown at 25HZ which is dominated by the misalignment peak at 20HZ for no fault case as shown in Figure 38. For 8 gram, 12 gram and 16 gram unbalance and misalignment peaks were observed at 1X and 2X rpm where the unbalance peak dominates the misalignment peaks as shown in Figure 39, Figure 40 and Figure 41. Similarly for Right Bearing Y-direction unbalance peak at 1X RPM is shown at 25HZ which is dominated by the misalignment peak at 20HZ for no fault case as shown in Figure 42. For 8 gram, 12 gram and 16 gram unbalance and misalignment peaks were observed at 1X and 2X rpm where the unbalance peak dominates the misalignment peaks as shown in Figure 43, Figure 44 and Figure 45.

AMPLITUDE SPECTRUM ANALYSIS (At RPM 300) LEFT BEARING X-DIERCTION (LX)

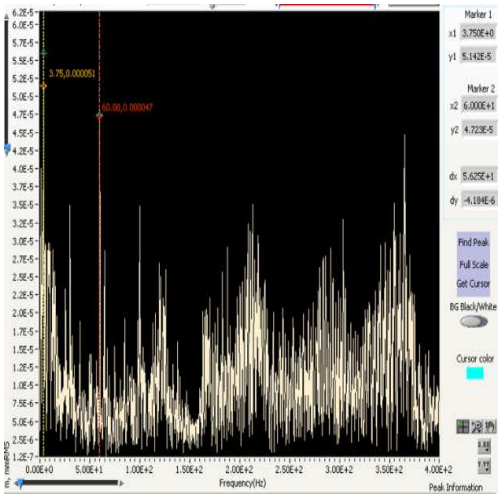

Figure 46: NFC300

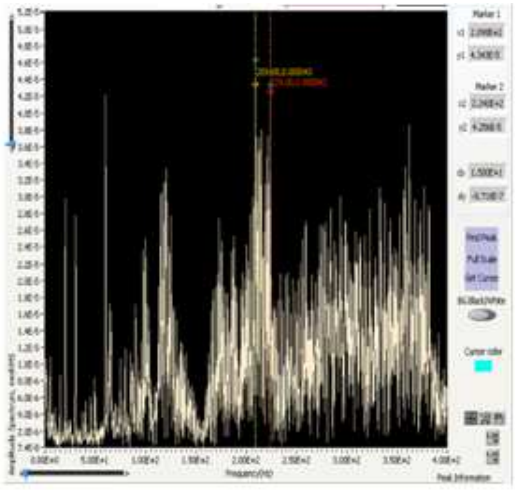

Figure 47: C8E1300

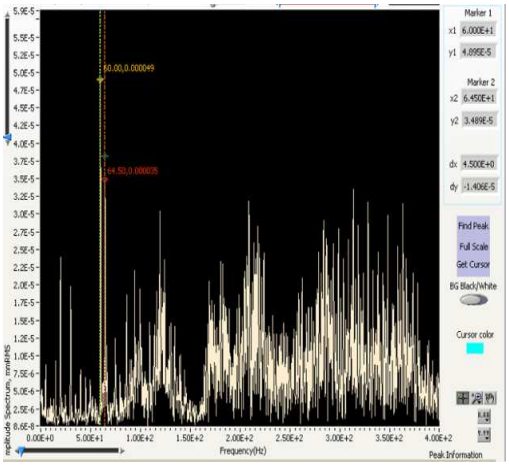

Figure 48: C12E1300

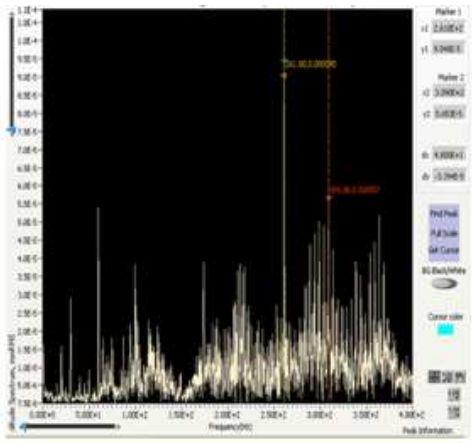

Figure 49: C16E1300

LEFT BEARING Y-DIRECTION (LY)

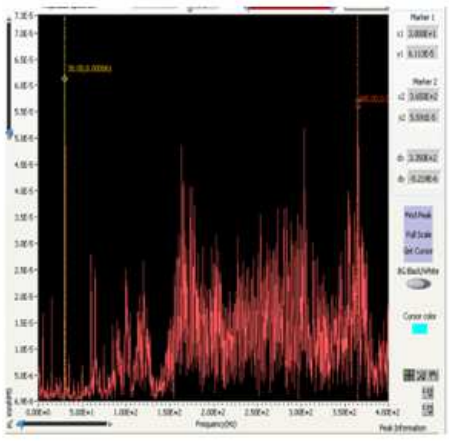

Figure 50: NFC300

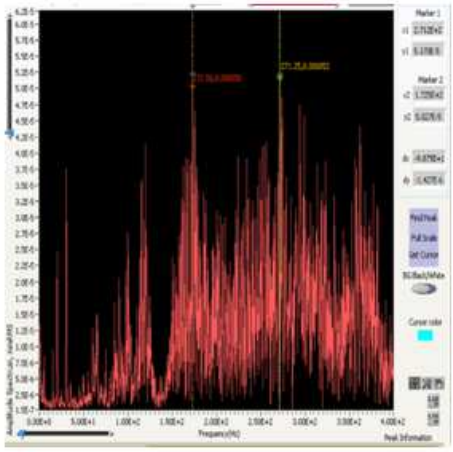

Figure 51: C8E1300

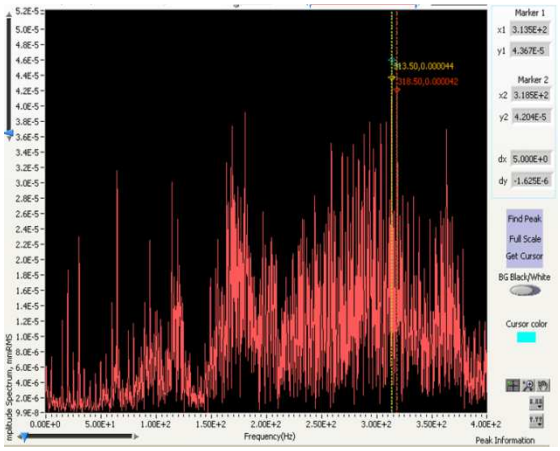

Figure 52: C12E1300

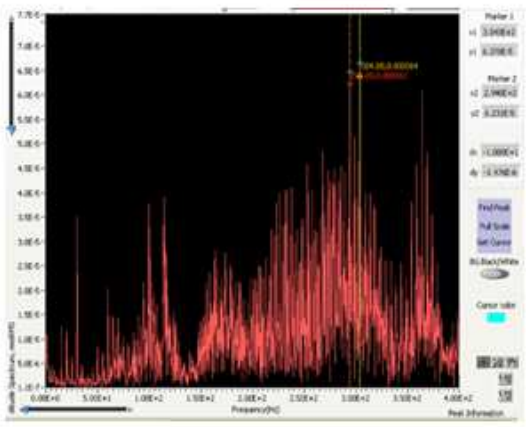

Figure 53: C16E1300

Amplitude Spectrum for Left Bearing X and Y direction at 300RPM has been shown in Figure 46 – Figure 47 for no fault case and unbalance mass of 8 gram, 12 gram and 16 gram respectively. From the spectrum analysis it can be concluded that amidst unbalance and misalignment fault, it's the bearing fault which is showing more no of dominant peaks at higher frequency.

RIGHT BEARING X-DIRECTION (RX)

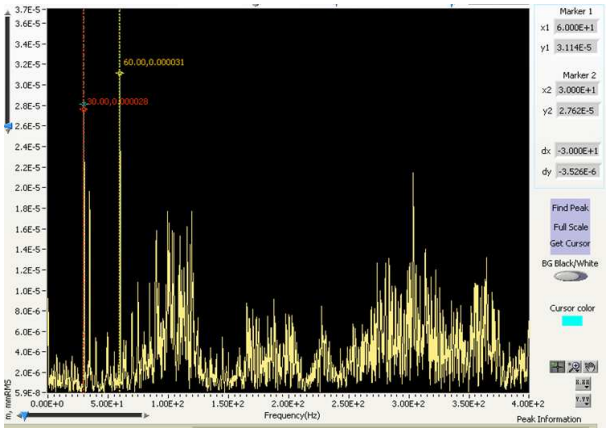

Figure 54: NFC300

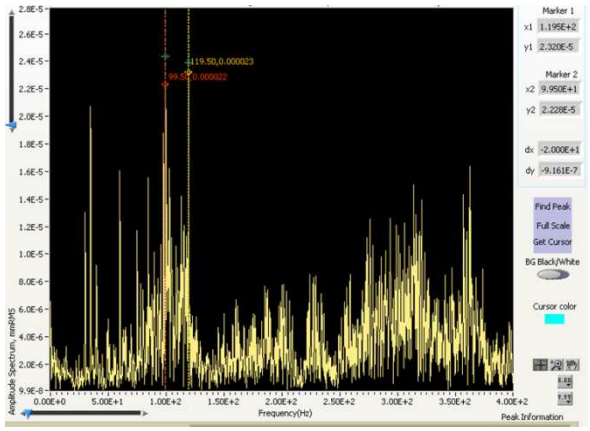

Figure 55:C8E1300

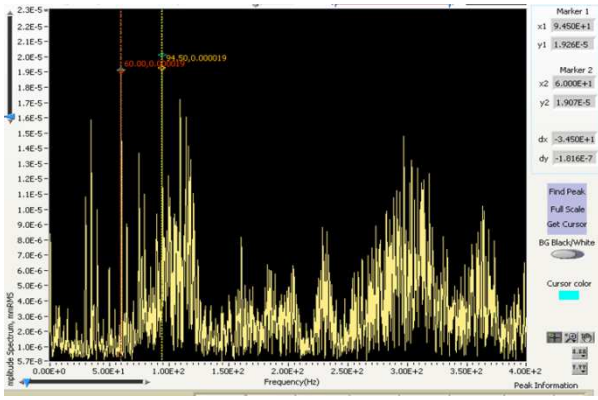

Figure 56: C12E1300

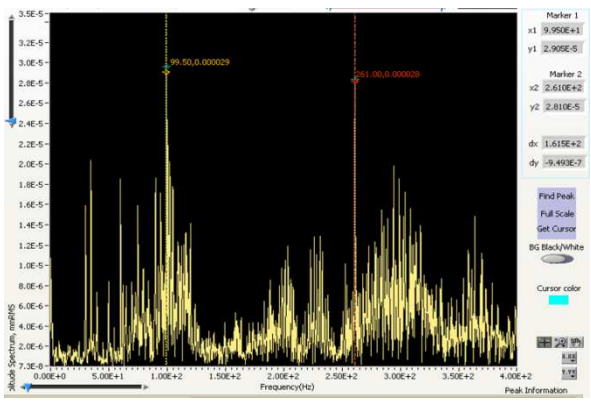

Figure 57: C16E1300

RIGHT BEARING Y-DIRECTION (RY)

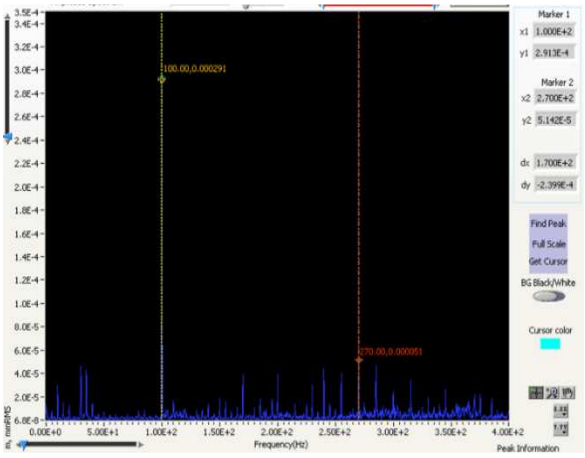

Figure 58: NFC300

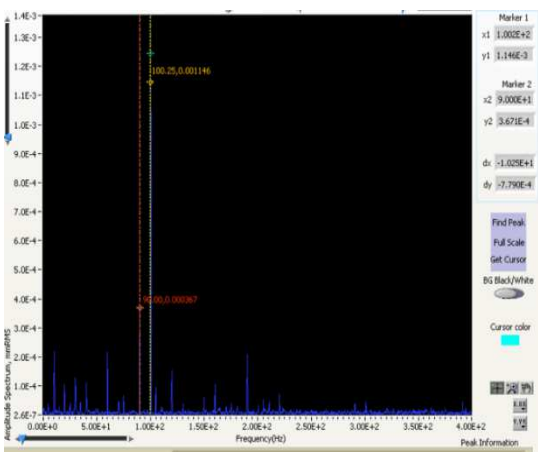

Figure 59: C8E1300

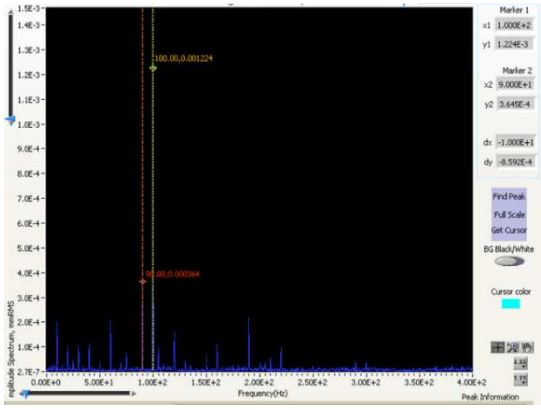

Figure 60: C12E1300

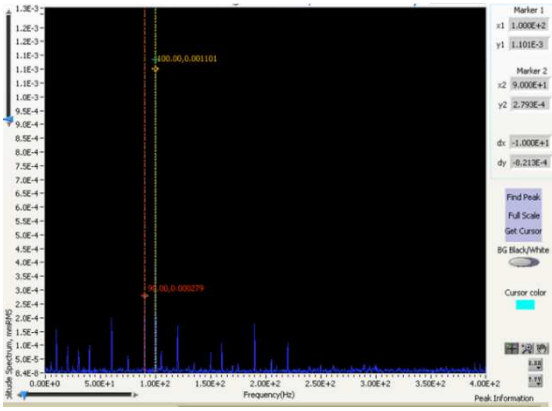

Figure 61: C16E1300

Amplitude Spectrum for Right Bearing X and Y direction at 300RPM has been shown in Figure 54 – Figure 55for no fault case and unbalance mass of 8 gram, 12 gram and 16 gram respectively. For Right Bearing X-direction bearing faults were predominant and was reflected accordingly in the amplitude spectrum In Right bearing Y direction there has been fewer bearing faults as compared to left bearing. Hence higher frequency peaks were observed less for right bearing amplitude spectrum in Y –direction. It has to be taken into account that the left bearing in this case appeared to be faultier than the right bearing in consideration.

(At RPM 1500)

LEFT BEARING X-DIERCTION (LX)

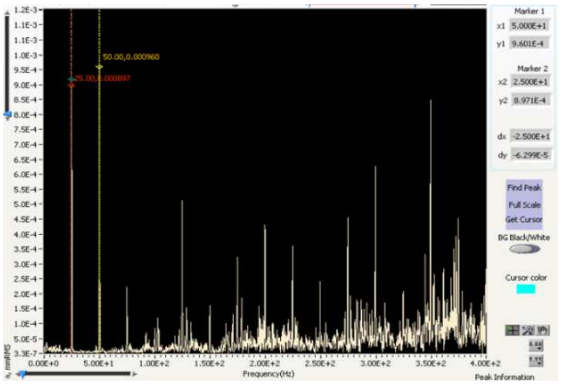

Figure 62: NFC1500

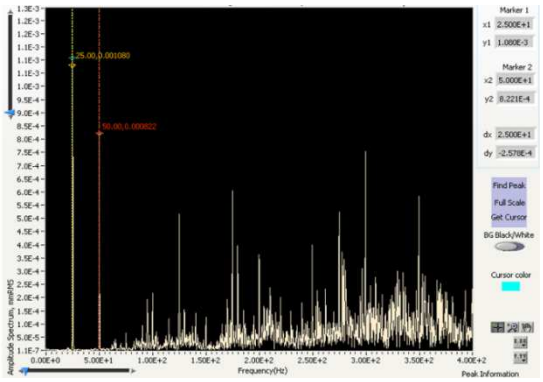

Figure 63: C8E11500

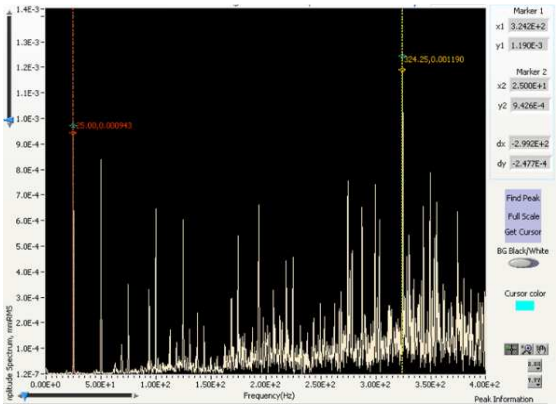

Figure 64: C12E11500

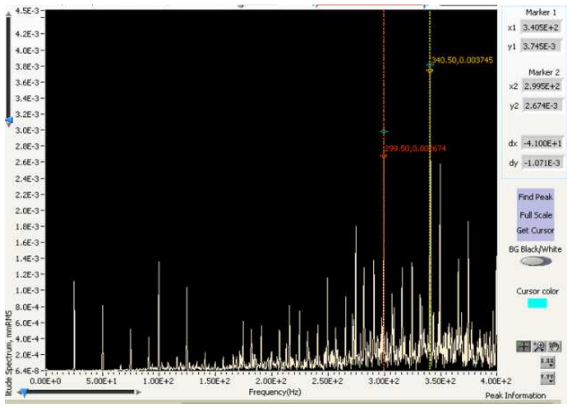

Figure 65: C16E11500

LEFT BEARING Y-DIERCTION (LY)

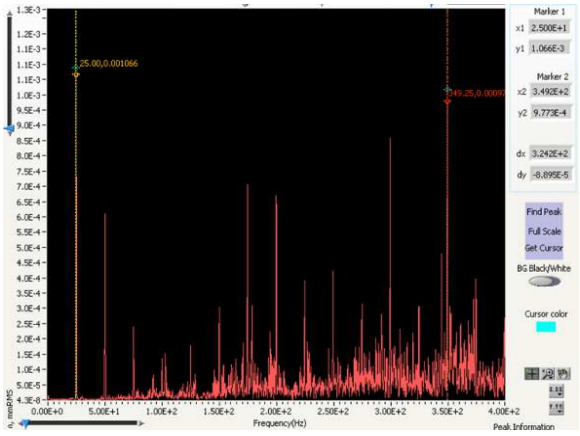

Figure 66: NFC1500

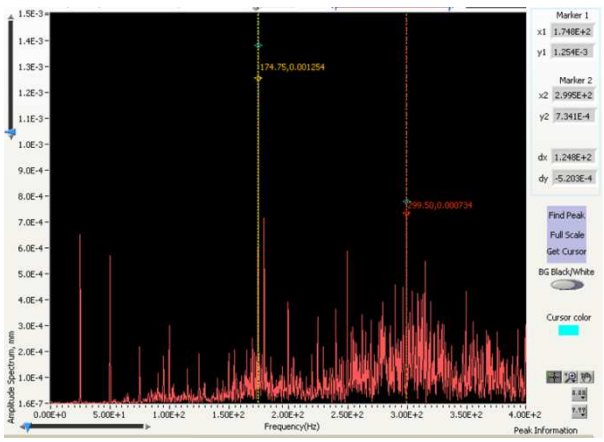

Figure 67: C8E11500

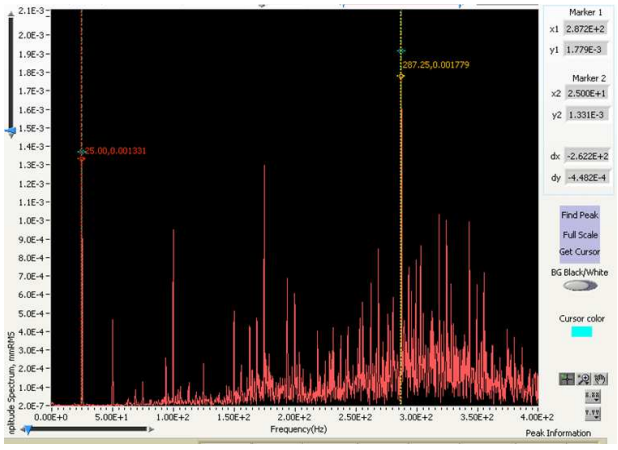

Figure 68: C12E11500

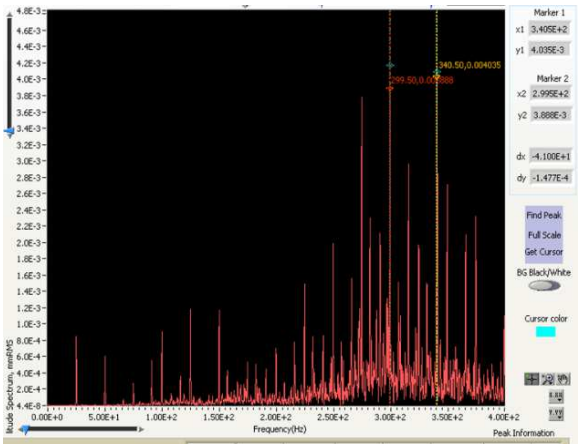

Figure 69: C16E11500

The amplitude spectrum shown in the Figure 68- Figure 69 is being represented for Left Bearing X and Y directions for 1500 RPM. It can be seen that unlike vibration spectrum at 300 RPM, the unbalance peaks at 1500 RPM are more prominent. Although frequency peaks due to bearing faults and other machine faults can be noticed, it is evident that unbalance and misalignment peaks are shown in the amplitude spectrum at higher RPM, though not predominant.

RIGHT BEARING X-DIERCTION (RX)

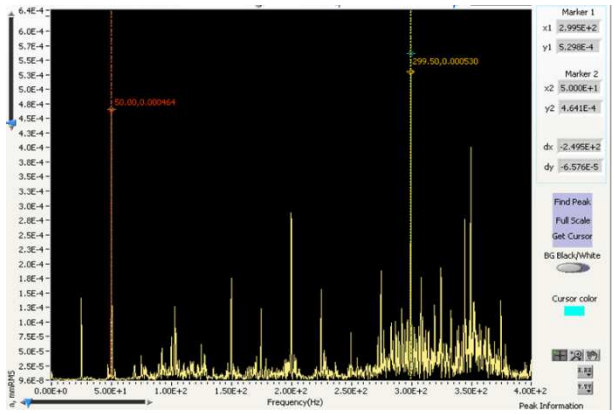

Figure 70: NFC1500

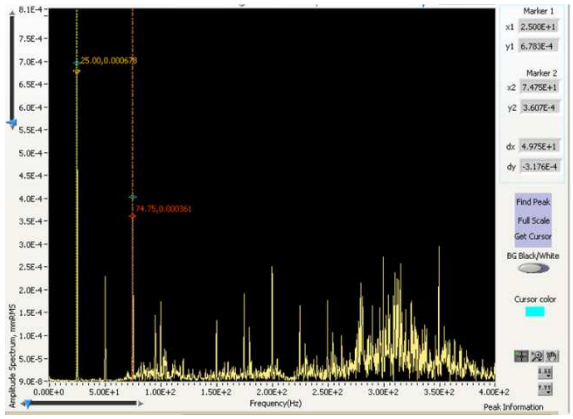

Figure 71: C8E11500

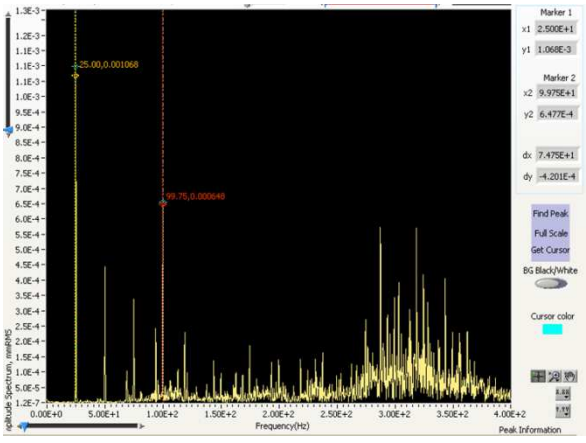

Figure 72: C12E11500

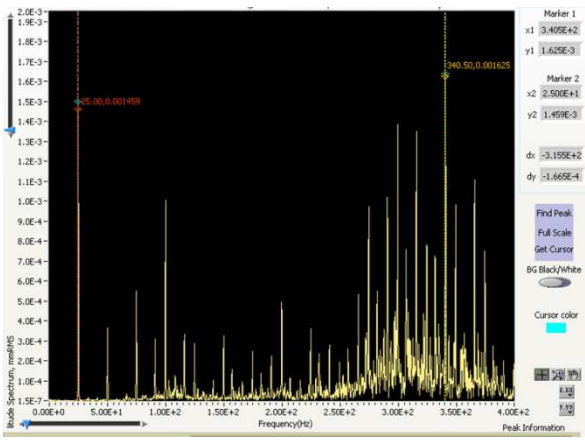

Figure 73: C16E11500

RIGHT BEARING Y-DIERCTION (RY)

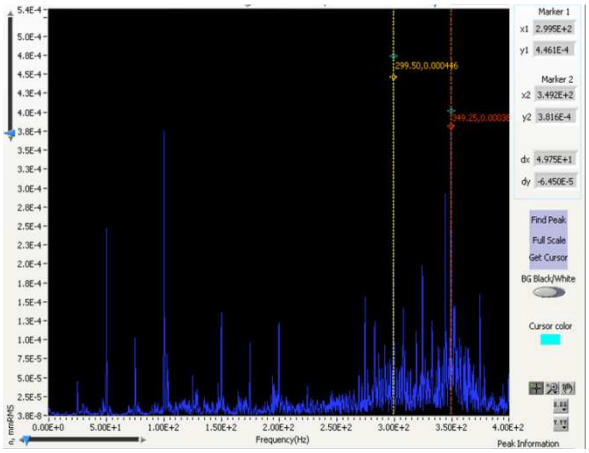

Figure 74: NFC1500

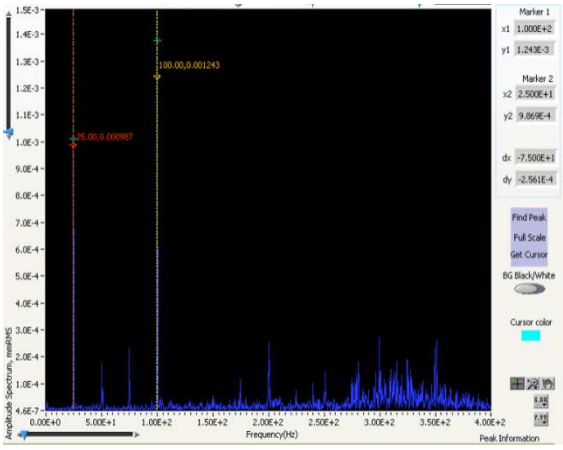

Figure 75: C8E11500

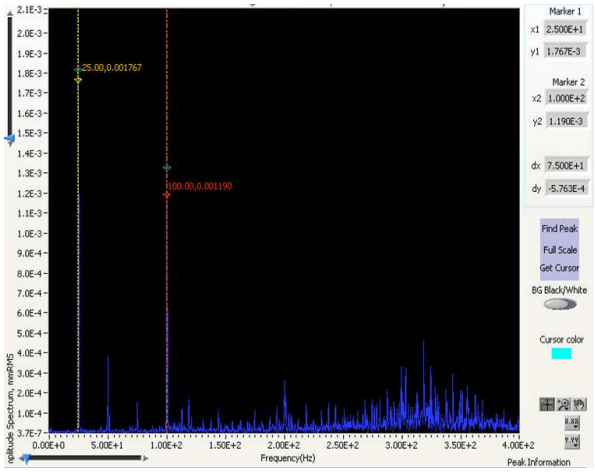

Figure 76: C12E11500

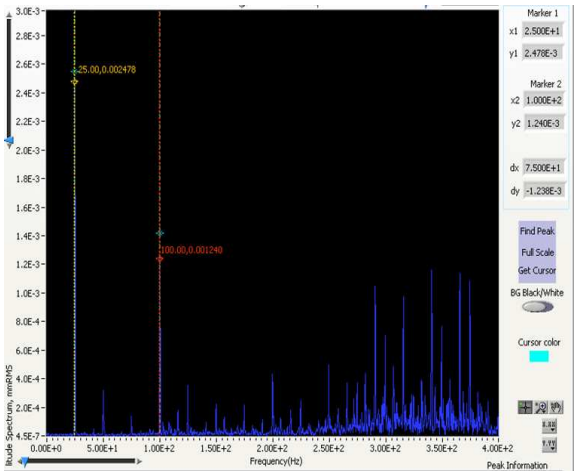

Figure 77: C16E11500

The amplitude spectrum shown in the Figure 76- Figure 77 is being represented for Right Bearing X and Y directions for 1500 RPM. Like previous cases of Left Bearing X and Y direction it can be seen that vibration spectrum at 1500 RPM showed prominent unbalance peaks which were not present at 300 RPM. Although frequency peaks due to bearing faults and other machine faults can be noticed, it is clear that unbalance and misalignment peaks are shown in the amplitude spectrum at higher RPM which are very dominant.

Table 2: Cross Power Spectrum Values for Different Settings

SL NO	EXP CODE	LEFT BEARING X-DIRECTION			LEFT BEARING Y-DIRECTION			RIGHT BEARING X-DIRECTION			RIGHT BEARING Y-DIRECTION		
		1ST PEAK	2ND PEAK	PHASE	1ST PEAK	2ND PEAK	PHASE	1ST PEAK	2ND PEAK	PHASE	1ST PEAK	2ND PEAK	PHASE
1	NFC300	5	10	258.69	5	30	31.31	30	34.75	338.51	10	30	170.52
	MAGNITUDE (LINEAR)	0.000086	0.000064		0.000049	0.000033		0.000015	0.000011		0.000063	0.000025	
2	C8E1300	5	30	93.6	5	30	161.83	5	34.75	181.71	10.25	30	275.23
	MAGNITUDE (LINEAR)	0.000032	0.000015		0.000025	0.000021		0.000009	0.000011		0.000173	0.000069	
3	C12E1300	5	15	104.83	5	15	106.16	5	34.75	285.55	5	10	160.1
	MAGNITUDE (LINEAR)	0.000026	0.00001		0.000022	0.000013		0.000011	0.000009		0.00009	0.000431	
4	C16E1300	30	59.75	200.97	15	30	41.45	30	34.75	82.55	5	10	347.29
	MAGNITUDE (LINEAR)	0.000015	0.000006		0.000014	0.000018		0.000008	0.000012		0.000115	0.000343	
5	NFC1500	25	50	315.49	25	50	166.79	25	50	87.81	25	50	182.66
	MAGNITUDE (LINEAR)	0.002617	0.001914		0.00311	0.001219		0.00041	0.000925		0.000133	0.000492	
6	C8E11500	25	50	319.77	25	50	166.19	25	50	94.34	25	50	177.17
	MAGNITUDE (LINEAR)	0.003205	0.001606		0.001886	0.001122		0.00197	0.000454		0.002866	0.000346	
7	C12E11500	25	50	263.57	25	50	89.03	25	50	49.32	25	50	76.03
	MAGNITUDE (LINEAR)	0.00311	0.001219		0.003858	0.000906		0.003095	0.000867		0.00512	0.000754	
8	C16E11500	25	50	172.94	25	274.45	41.27	25	50	337.11	25	50	63.13
	MAGNITUDE (LINEAR)	0.001886	0.001122		0.00244	0.001375		0.004201	0.000721		0.007136	0.000624	

Table 3: Amplitude Spectrum True Peak Values for Different Settings

SL NO	EXP CODE	LEFT BEARING X-DIRECTION			LEFT BEARING Y-DIRECTION			RIGHT BEARING X-DIRECTION			RIGHT BEARING Y-DIRECTION		
		1ST PEAK	2ND PEAK	PHASE	1ST PEAK	2ND PEAK	PHASE	1ST PEAK	2ND PEAK	PHASE	1ST PEAK	2ND PEAK	PHASE
1	NFC300	3.805	60	258.69	30.015	364.989	31.31	30.039	60.006	338.51	99.976	270.017	170.52
	Amplitude (mm) RMS	5.60E-05	4.72E-05		6.16E-05	5.72E-05		2.81E-05	3.12E-05		2.92E-04	5.17E-05	
2	C8E1300	209	224.018	93.6	172.54	271.218	161.83	99.603	119.453	181.71	90.007	100.341	275.23
	Amplitude (mm) RMS	4.68E-05	4.33E-05		5.23E-05	5.22E-05		2.44E-05	2.39E-05		3.67E-05	1.25E-03	
3	C12E1300	59.992	64.575	104.83	313.478	318.463	106.16	59.992	94.39	285.55	89.999	99.982	160.1
	Amplitude (mm) RMS	4.91E-05	3.82E-05		4.60E-05	4.52E-05		1.91E-05	2.01E-05		3.65E-04	1.23E-03	
4	C16E1300	260.997	308.996	200.97	294.031	304.027	41.45	99.516	260.996	82.55	90.003	99.945	347.29
	Amplitude (mm) RMS	9.46E-05	5.69E-05		6.47E-05	6.65E-05		2.96E-05	2.83E-05		2.79E-04	1.14E-03	
5	NFC1500	24.953	49.997	315.49	24.954	349.308	166.79	50.02	299.433	87.81	299.418	349.323	182.66
	Amplitude (mm) RMS	9.18E-04	9.60E-04		1.09E-03	1.02E-03		4.65E-04	5.62E-04		4.74E-04	4.01E-04	
6	C8E11500	24.949	50.005	319.77	174.656	299.418	166.19	24.95	74.846	94.34	24.952	100.091	177.17
	Amplitude (mm) RMS	1.11E-03	8.22E-04		1.38E-03	7.77E-04		6.96E-04	4.03E-04		1.01E-03	1.38E-03	
7	C12E11500	24.947	324.315	263.57	24.947	287.345	89.03	24.947	99.784	49.32	24.948	100.073	76.03
	Amplitude (mm) RMS	9.70E-04	1.24E-03		1.37E-03	1.91E-03		1.10E-03	6.56E-04		1.82E-03	1.33E-03	
8	C16E11500	299.4	340.461	172.94	299.416	340.467	41.27	24.949	340.478	337.11	24.949	100.068	63.13
	Amplitude (mm) RMS	2.98E-03	3.82E-03		4.17E-03	4.09E-03		1.50E-03	1.64E-03		2.55E-03	1.42E-03	

In the above Table 2 and Table 3, values of amplitude spectrum and cross power spectrum has been presented. The 1st peak and the 2nd Peak values corresponds to the first two higher peaks values and their corresponding frequencies.

Also the phase value for different readings measured in degrees has been noted down. These values are compared and analysed using an ORIGIN software.

Comparison of Result between Cross Power Spectrum and Amplitude Spectrum

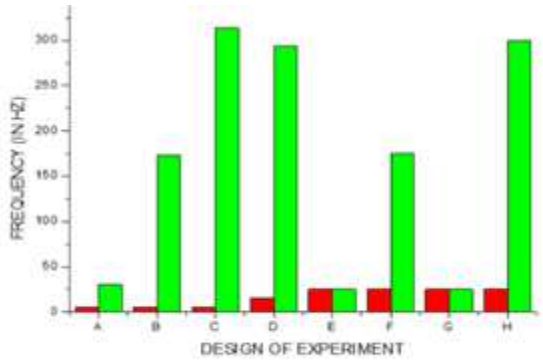

Figure 78: Left Bearing X-Direction

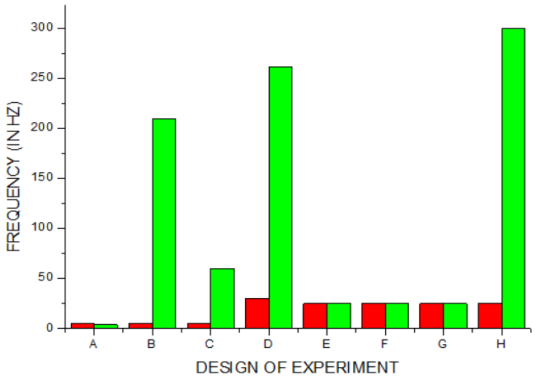

Figure 79: Left Bearing Y-Direction

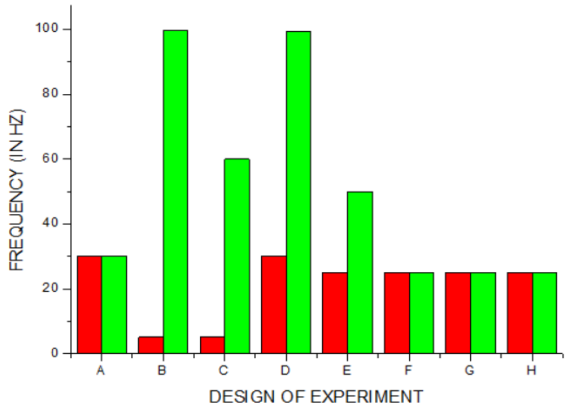

Figure 80: Right Bearing X-Direction

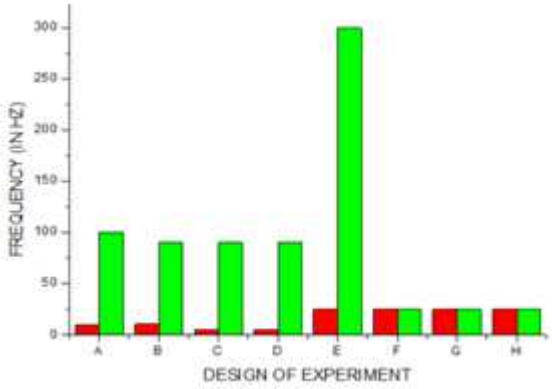

Figure 81: Right Bearing Y-Direction

- Frequency in Hertz for Amplitude Spectrum

- Frequency in Hertz for Cross Power Spectrum

Legends

A – NFC300, **B** – C8E1300,**C** – C12E1300, **D** - C16E1300, **E**- NFC1500, **F** – C8E11500,**G** – C12E11500**H** – C16E11500

A comparative analysis has been done between the Cross Power spectrum and the Amplitude spectrum for frequency domain analysis of various states of the machine subjected to different faults. The accuracy level depends upon the calibration of the accelerometer in use.

The red bars in the figures above indicate the frequency in hertz for the Amplitude spectrum whereas the green bar indicates the frequency in hertz for the Cross power spectrum. At lower RPM (300), the frequency peaks of cross power spectrum and the amplitude spectrum showed significant differences. Whereas similar results were obtained at higher RPM (1500). Also no noise interference was observed in cross power spectrum analysis. Although noise filters were

used before data collection, there has been significant noise interference in the amplitude spectrum due to which frequency peaks were not obtained as desired.

CONCLUSIONS AND FUTURE SCOPE OF WORK

It has been noticed that the cross power spectrum and the amplitude spectrum reflected similar results at higher RPM (at 1500 RPM) rather than at lower 300RPM. Hence it can be concluded that the RPM of the shaft has a major effect on the unbalance vibration features the most yielding the frequency domain characteristics than the unbalance mass or eccentricity. Also the cross power spectrum revealed more accurate result than the amplitude spectrum in consideration for the same input conditions. Frequency peak dominancy is a subject of speed of shaft which can be easily predicted using a cross power spectrum.

The same work can be extended for with two or more no of discs mounted on the shaft and more no of unbalance features added to the system. Also other faults like misalignment and bearing faults can be added to the system leading to multi fault system.

ACKNOWLEDGEMENTS

The author is thankful to the Department of Mechanical Engineering, National Institute of Technology Durgapur and Condition Monitoring and Structural Analysis Group of Central Mechanical Engineering Research Institute located at Durgapur to help me to carry out this work on “Comparative Spectrum Analysis for vibration in a rotating machine with multiple varying conditions for unbalance fault and check for frequency peak dominancy”.

REFERENCES

1. *Jae Hong Suh, Soundar R. T. Kumara (I), Shreesh P. Mysore, (2004)Machinery Fault Diagnosis and Prognosis: Application of Advanced Signal Processing Techniques, Annals of the ClRP Vol. 48/7/7999 317.*
2. *Peter W. Tse, Wen-Xian Yang, H.Y. Tam, (2004) Machine fault diagnosis through an effective exact wavelet analysis, Journal of Sound and Vibration 277 1005–1024.*
3. *D.F. Shi, F. Tsung, P.J. Unsworth, (2004) Adaptive time–frequency decomposition for transient vibration monitoring of rotating machinery, Mechanical Systems and Signal Processing 18 127–141.*
4. *Je ro me Antoni, R.B. Randall, (2006) The spectral kurtosis: application to the vibratory surveillance and diagnostics of rotating machines, Mechanical Systems and Signal Processing 20 308–331.*
5. *H.X. Chen, Patrick S.K. Chua, G.H. Lim, (2006)Adaptive wavelet transform for vibration signal modelling and application in fault diagnosis of water hydraulic motor, Mechanical Systems and Signal Processing 20 2022–2045*
6. *Qiang Miao, Viliam Makis,(2007) Condition monitoring and classification of rotating machinery using wavelets and hidden Markov models, Mechanical Systems and Signal Processing 21 40–855.*
7. *Rui Zhou, Wen Bao, Ning Li, Xin Huang, Daren Yu, (2010) Mechanical equipment fault diagnosis based on redundant second generation wavelet packet transform, Digital Signal Processing 20 276–288.*
8. *J. Cusido, L. Romeral, J.A. Ortega, A. Garcia, J.R. Riba, (2010) Wavelet and PDD as fault detection techniques, Electric Power Systems Research 80 915–924.*
9. *Yanxue Wang, Zhengjia He, Yanyang Zi, (2010)Enhancement of signal denoising and multiple fault signatures detecting in rotating machinery using dual-tree complex wavelet transform, Mechanical SystemsandSignalProcessing24119–137.*

10. *F. Al-Badour, M.Sunar, L.Cheded, (2011) Vibration analysis of rotating machinery using time–frequency analysis and wavelet techniques, Mechanical SystemsandSignalProcessing252083–2101.*
11. *Lei You, Jun Hu, Fang Fang, Lintao Duan, (2011)Fault diagnosis system of rotating machinery vibration signal, Procedia Engineering 15 671 – 675.*
12. *Shibin Wang, Weiguo Huang, Z.K. Zhu, (2011) Transient modeling and parameter identification based on wavelet and correlation filtering for rotating machine fault diagnosis, Mechanical SystemsandSignalProcessing251299–1320.*
13. *Z.K Peng, W.M Zhang, Z.Q Lang, G.Meng, F.L Chu, (2012) Time–frequency data fusion technique with application to vibration signal analysis, Mechanical Systems and Signal Processing29164–173.*
14. *Md. Abdul Saleem, G. Diwakar, Dr. M.R.S. Satyanarayana, (Sep-Oct. 2012), Detection of Unbalance in Rotating Machines Using Shaft Deflection Measurement during Its Operation, IOSR Journal of Mechanical and Civil Engineering (IOSR-JMCE) ISSN: 2278-1684 Volume 3, Issue 3 PP 08-20.*
15. *B. Kiran Kumar, G. Diwakar, Dr. M. R. S. Satynarayana, (Sep-Oct. 2012)Determination of Unbalance in Rotating Machine Using Vibration Signature Analysis, International Journal of Modern Engineering Research (IJMER),Vol.2, Issue.5, pp-3415-3421 ISSN: 2249-6645.*
16. *Bin Qiang Chen, Zhou Suo Zhang, Yan Yang Zi, Zheng Jia He, Chuang Sun, (2013)Detecting of transient vibration signatures using an improved fast spatial–spectral ensemble kurtosis kurtogram and its applications to mechanical signature analysis of short duration data from rotating machinery, Mechanical SystemsandSignalProcessing401–37*
17. *Jun Wang, Qingbo He, Fanrang Kong, (2013)Automatic fault diagnosis of rotating machines by time-scale manifold ridge analysis, Mechanical SystemsandSignalProcessing40237–256.*
18. *Qingbo He, Xiangxiang Wang, (2013),Time–frequency manifold correlation matching for periodic fault identification in rotating machines, Journal of Sound and Vibration3322611–2626.*
19. *Dongju Chen, Jinwei Fan, Feihu Zhang, (2013) Extraction the unbalance features of spindle system using wavelet transform and power spectral density, Measurement 46 1279–1290*
20. *Chen Bin Qiang, Zhang Zhou Suo, Zi Yan Yang, Yang Zhi Bo & He Zheng Jia, (May 2013),A pseudo wavelet system-based vibration signature extracting method for rotating machinery fault detection, Science China Technological Sciences, Vol.56 No.5: 1294–1306.*
21. *M. Lokesha, Manik Chandra Majumder, K. P. Ramachandran, Khalid Fathi Abdul Raheem, (2014)Fault Detection and Diagnosis in gears using wavelet enveloped power spectrum and ANNIJRET: International Journal of Research in Engineering and Technology e ISSN: 2319-1163 | p ISSN: 2321-7308*
22. *Shibin Wang, Gaigai Cai, Zhongkui Zhu, Weiguo Huang, Xingwu Zhang,(2015) Transient signal analysis based on Levenberg–Marquardt method for fault feature extraction of rotating machines, Mechanical SystemsandSignalProcessing54-5516–40*
23. *Y. Yang, X.J.Dong, Z.K.Peng, W.M.Zhang, G.Meng, (2015) Vibration signal analysis using parameterized time–frequency method for features extraction of varying-speed rotary machinery, Journal ofSoundandVibration335 350–366.*
24. *Adrian D.Nembhard, Jyoti K. Sinha, A.Yunusa-Kaltungo, (2015) Development of a generic rotating machinery fault diagnosis approach insensitive to machine speed and support type, Journal ofSoundandVibration337 321–341*
25. *Wei Li, Zhencai Zhu, Fan Jiang, Gongbo Zhou, Guoan Chen, (2015) Fault diagnosis of rotating machinery with a novel statistical feature extraction and evaluation method, Mechanical SystemsandSignalProcessing50-51 414–426*

26. *Hocine Bendjama, Mohamad S. Boucherit, Saleh Bouhouche, (2015)Fault Diagnosis of rotating Machinery using wavelet transform and principal component analysis, Unitée de Recherche Appliquée en Sidérurgie et Métallurgie URASM-CSC, BP 196 Site Sidérurgiqued'El-hadjar, Annaba, Algérie, Département de génieélectrique et automatique, Ecole Nationale Polytechnique ENP,10 Hassen Badi, BP 182 El-Harrach, Alger, Algérie.*

27. *Phadatare H. P., Barun Pratiher, (2016) Nonlinear Frequencies and Unbalanced Response Analysis of High Speed Rotor-Bearing Systems, Procedia Engineering 144 801 – 809.*